Cell. Mol. Life Sci. (2018) 75:1461–1482
https://doi.org/10.1007/s00018-017-2699-2

Cellular and Molecular Life Sciences

ORIGINAL ARTICLE

Characterizations of PMCA2-interacting complex and its role as a calcium oxalate crystal-binding protein

Arada Vinaiphat[1,2] · **Visith Thongboonkerd**[1,2]

Received: 11 August 2017 / Revised: 24 October 2017 / Accepted: 26 October 2017 / Published online: 30 October 2017

Abstract Three isoforms of plasma membrane Ca^{2+}-ATPase (PMCA) are expressed in the kidney. While PMCA1 and PMCA4 play major role in regulating Ca^{2+} reabsorption, the role for PMCA2 remains vaguely defined. To define PMCA2 function, PMCA2-interacting complex was characterized by immunoprecipitation followed by nanoLC-ESI-Qq-TripleTOF MS/MS (IP-MS). After subtracting non-specific binders using isotype-controlled IP-MS, 474 proteins were identified as PMCA2-interacting partners. Among these, eight were known and 20 were potential PMCA2-interacting partners based on bioinformatic prediction, whereas other 446 were novel and had not been previously reported/predicted. Quantitative immuno-co-localization assay confirmed the association of PMCA2 with these partners. Gene ontology analysis revealed binding activity as the major molecular function of PMCA2-interacting complex. Functional validation using calcium oxalate monohydrate (COM) crystal-protein binding, crystal-cell adhesion, and crystal internalization assays together with neutralization by anti-PMCA2 antibody compared to isotype-controlled IgG and blank control, revealed a novel role of PMCA2 as a COM crystal-binding protein that was crucial for crystal retention and uptake. In summary, a large number of novel PMCA2-interacting proteins have been defined and a novel function of PMCA2 as a COM crystal-binding protein sheds light onto its involvement, at least in part, in kidney stone pathogenesis.

Keywords Crystal adhesion · Crystal internalization · Immuno-co-localization · Interactomics · IP-MS · Kidney stone · Renal calculi · Renal tubular cells

Introduction

Plasma membrane Ca^{2+}-ATPase (PMCA) is a P-type ion-transporting ATPase that plays a major role in regulating Ca^{2+} balance in various types of eukaryotic cells [1]. Activation of this protein requires binding of Ca^{2+}-dependent calmodulin to its C-terminal tail [2], while many other mechanisms, i.e., phosphorylation, phospholipid activation and proteolysis can also affect PMCA activity [3–5]. At present, four PMCA isoforms (PMCA1–4) with more than 30 modified forms generated by alternative RNA splicing have been reported [6, 7]. Such diversity in spliced regions is responsible for their unique membrane localizations and dynamic Ca^{2+} handling activities. The role of PMCA is becoming more relevant as growing numbers of evidence have demonstrated that PMCA abnormalities can lead to dysfunction of mammalian cells both in vitro [8] and in vivo [9–11].

In the kidney, expression of PMCA1, PMCA2 and PMCA4 has been found at both RNA and protein levels [12, 13]. PMCA1 and PMCA4, which are designated as "housekeeping" PMCA, are highly expressed at basolateral membranes of renal tubular cells, and hence are considered as the major forms responsible for 1/3 of Ca^{2+} reabsorption along the nephron [whereas the remainders are governed

Electronic supplementary material The online version of this article (https://doi.org/10.1007/s00018-017-2699-2) contains supplementary material, which is available to authorized users.

✉ Visith Thongboonkerd
thongboonkerd@dr.com; vthongbo@yahoo.com

[1] Medical Proteomics Unit, Office for Research and Development, Faculty of Medicine Siriraj Hospital, Mahidol University, 6th Floor-SiMR Building, 2 Wanglang Road, Bangkoknoi, Bangkok 10700, Thailand

[2] Center for Research in Complex Systems Science, Mahidol University, Bangkok, Thailand

by Na^+/Ca^{2+} exchanger (NCX)] [14]. In contrast, PMCA2 isoform has been found with a much lower level but without restriction to specific membrane compartment [15, 16]. Moreover, two important properties that set apart PMCA2 from the other two isoforms are that the rate of stimulus and Ca^{2+}-binding affinity is considerably much higher [7, 17]. While PMCA1 and PMCA4 play a major role in regulating Ca^{2+} reabsorption, the role of PMCA2 remains vaguely defined (perhaps due to its low abundant expression). These distinctive features and conservation of PMCA2 in renal cells through evolutionary adaptation have thus come to our attention as PMCA2 may have unique function, rather than functional redundancy in controlling Ca^{2+} reabsorption [17–19].

To explore functions and regulatory mechanisms of a target protein in a given cell, characterizations of its interacting complex is one of the essential approaches [20]. We, therefore, performed extensive characterizations of PMCA2-interacting partners in renal tubular cells by a combination of immunoprecipitation and mass spectrometry (IP-MS). Quantitative immuno-co-localization assay was performed to confirm the association of PMCA2 with its partners. Finally, functional investigations of PMCA2 were performed using calcium oxalate monohydrate (COM) crystal-protein binding, crystal-cell adhesion, and crystal internalization assays, together with neutralization by specific antibody against PMCA2 compared to isotype-controlled IgG and blank control.

Materials and methods

Cell culture

Madin–Darby canine kidney (MDCK) cell line, which was originally derived from the distal nephron segment [21], was cultivated under standard condition in Eagle's minimum essential medium (MEM) (Gibco; Grand Island, NY, USA) supplemented with 10% heat-inactivated fetal bovine serum (FBS) (Gibco), 1.2% penicillin G/streptomycin, and 2 mM L-glutamine (Sigma; St. Louis, MO, USA) in a humidified incubator at 37 °C and 5% CO_2.

Affinity purification by immunoprecipitation (IP)

MDCK cells were lyzed in a modified RIPA buffer (50 mM Tris–HCl (pH 7.4), 150 mM NaCl, 0.5% Triton X-100, and 1 mM EDTA) and further homogenized by sonication. Cell debris and particulate matters were removed by centrifugation at 10,000×*g* and 4 °C for 15 min. Prior to IP, 3 mg of cell lysate were pre-cleared with 50 µl of protein G Sepharose beads (50% slurry) at 4 °C on a rotary device for 15 min. Beads with non-specifically bounded proteins were removed by centrifugation at 1500×*g* and 4 °C for 5 min. Thereafter, the sample was incubated with 1 µg of rabbit polyclonal anti-PMCA2 antibody (Abcam; Cambridge, UK) or 1 µg of isotype-controlled rabbit IgG (Santa Cruz Biotechnology; Santa Cruz, CA, USA) overnight at 4 °C on a rotary device. Protein G Sepharose beads (50 µl) were then added and incubated with each mixture at 4 °C for 4 h. Thereafter, the beads were collected by centrifugation at 1500×*g* and 4 °C for 5 min and washed five times with 800 µl modified RIPA buffer. The immunoprecipitated proteins were finally eluted from the beads using Laemmli's buffer and subjected to mass spectrometric identification and SDS-PAGE, in which protein bands were visualized using Oriole fluorescent gel stain (Bio-Rad Laboratories; Hercules, CA, USA). Gel images were acquired with a ChemiDoc MP System (Bio-Rad Laboratories).

In-gel tryptic digestion and identification of proteins by nanoLC-ESI-Qq-TripleTOF MS/MS

Each lane of the SDS-PAGE gel was excised into 20 slices/lane. The gel slices were subjected to in-gel tryptic digestion as described previously [22, 23]. Analysis of the digested peptides was performed using reversed-phase Eksigent Ultra Plus nano-LC 2D HPLC system (Eksigent; Dublin, CA, USA) coupled to the new generation quadrupole time-of-flight (QqTOF) Triple TOF 5600 mass spectrometer (AB SCIEX; Concord, Canada). For LC system, mobile phase A was 2% acetonitrile (ACN)/0.1% formic acid, and mobile phase B was 98% ACN/0.1% formic acid. Samples were loaded using autosampler and desalted using a nanoLC Trap (ChromXP C18-CL, 350 µm I.D. × 0.5 mm, 3 µm particle size, 120 Å pore size) (Eksigent) at a flow rate of 3 µl/min using isocratic 100% mobile phase A for 8 min. After pre-washing, the samples were transferred onto the analytical C18-nanocapillary HPLC column (ChromXP C18-CL, 75 µm I.D. × 15 cm, 3 µm particle size, 120 Å pore size) (Eksigent) and eluted at a flow rate of 300 nl/min. Peptides were separated using a linear and stepwise gradient of 5–40% mobile phase B over 40 min, 40–50% B over 5 min, 60–80% B over 1 min, and 80% B over 10 min, with a total runtime of 70 min including mobile phase equilibration. MS and MS/MS spectra were acquired in positive-ion and high-sensitivity mode with a resolution of ~ 35,000 full width half maximum. The data were acquired using a nanospray needle voltage of 2.4 kV, curtain gas of 30 psi, nebulizer gas of 8 psi, an interface heater temperature of 150 °C. The precursor ions were fragmented in a collision cell using nitrogen as the collision gas with the collision energy setting of 30 ± 13 for induction of CID. Advanced information dependent acquisition (IDA) was used for MS/MS collection on the Triple TOF 5600 to obtain MS/MS spectra for the 20 most abundant precursor ions following each survey MS1

scan. The charge state of + 2 and + 3 of precursor and product ions was collected. Exclusion of former target ions was set for 6 s after 1 occurrence. Raw.wiff file was converted to the searchable.mgf file using MS Data Converter (AB SCIEX) for independent searches using the Mascot software version 2.4.0 (Matrix Science; London, UK) to query against the Uniprot-SwissProt mammalian protein database. Fixed modification was carbamidomethylation at cysteine residues, whereas variable modification was oxidation at methionine residues. Only one missed trypsin cleavage was allowed, and peptide mass tolerances of 50 ppm and 0.4 Da were allowed for MS/MS ions search. The target false discovery rate (FDR) was analyzed by performing a concatenated decoy database search and the identified proteins are reported at FDR < 1%.

Bioinformatics analysis

Proteins that were present exclusively in the anti-PMCA2-IP sample were further analyzed by Search Tool for the Retrieval of Interacting Genes/Proteins (STRING) version 10 (http://www.string-db.org) for their interaction networks. Functional classification was performed using Protein ANalysis THrough Evolutionary Relationships (PANTHER) software (http://pantherdb.org/).

Quantitative immuno-co-localization assay

The cell monolayer was cultivated on coverslips and washed three times with ice-cold membrane preserving buffer (1 mM $MgCl_2$ and 0.1 mM $CaCl_2$ in PBS) prior to fixation with 4% paraformaldehyde at room temperature (set at 25 °C) for 15 min. After washing with PBS, the cells were permeabilized with 0.1% Triton X-100 at room temperature for 15 min and non-specific bindings were blocked with 1% BSA in PBS for 30 min. The cells were then incubated at 37 °C for 1 h with rabbit polyclonal anti-PMCA2 (Abcam) together with each of the following primary antibodies: mouse monoclonal anti-ezrin (Santa Cruz Biotechnology), anti-Na^+/K^+-ATPase (Santa Cruz Biotechnology), anti-annexin A1 (Chemicon; Temecula, CA, USA), anti-Alix (Santa Cruz Biotechnology), anti-nhRNP K (Santa Cruz Biotechnology), anti-c-Jun (Santa Cruz Biotechnology), anti-SOD-1 (Santa Cruz Biotechnology), and anti-DJ-1 (Santa Cruz Biotechnology) (all were diluted 1:50 in 1% BSA/PBS). For actin staining, Alexa488-conjugated phalloidin (Invitrogen-Molecular Probes; Eugene, OR, USA) was used instead. After rinsing with PBS, the cells were then incubated with Alexa546-conjugated goat anti-rabbit IgG and Alexa488-conjugated goat anti-mouse IgG secondary antibodies (Invitrogen-Molecular Probes) containing 0.1 g/ml Hoechst dye (Sigma) at 37 °C for 1 h. Finally, the cells were washed with PBS and mounted onto slides with 50% glycerol/PBS for subsequent examination under ECLIPSE Ti-Clsi4 Laser Unit (Nikon; Tokyo, Japan).

Fluorescence intensity profiles were generated using NIS-Elements D v.4.11 imaging software (Nikon). A linear section of area of interest with a distance of 15 µm was manually drawn across the cell from left to right borders and the intensity profiles were obtained from each color channel. Pixel-to-pixel frequency scatter plots were generated with WCIF ImageJ bundle plugins in ImageJ software (https://imagej.nih.gov/). Pearson's correlation coefficient (r) values were obtained from the JACoP plugin [24] and r values with $p < 0.05$ that were considered as valid co-localization of the two signals [25].

Preparation of plain and fluorescence-labeled calcium oxalate monohydrate (COM) crystals

Plain and fluorescence-labeled COM crystals were generated as described previously [26–29]. The plain crystals were prepared by mixing 500 ml of solution A (10 mM $CaCl_2{\cdot}2H_2O$ in 10 mM Tris–HCl and 90 mM NaCl, pH 7.4) and 500 ml of solution B (1 mM $Na_2C_2O_4$ in 10 mM Tris–HCl and 90 mM NaCl, pH 7.4). After an overnight incubation, COM crystals were collected and washed with absolute methanol, left to air dry, and sterilized under UV-light prior to COM crystal-protein binding and crystal-cell adhesion assays. To prepare fluorescence-labeled COM crystals, 0.01 µg/ml fluorescein isothiocyanate (FITC) dye (Thermo Scientific Pierce; Rockford, IL, USA) was added to solution A prior to the addition of solution B as described above. After an overnight incubation in the dark, the FITC-labeled COM crystals were then collected and treated the same way as for the plain crystals prior to crystal internalization assay.

Isolation of apical membranes

Apical membranes were isolated from the polarized MDCK cells using a peeling method as described previously [30, 31]. Briefly, Whatman filter paper (0.18-mm-thick, Whatman International Ltd.; Maidstone, UK) pre-wetted with deionized water was placed onto the cell monolayer. After 5-min incubation, the filter paper was peeled out and the apical membranes retained under the filter paper surface were harvested by rehydration in deionized water and gentle scrapping. The apical membrane-enriched fraction was then lyophilized. Dried apical membranes were solubilized in Laemmli's buffer and quantitated by Bradford's method using Bio-Rad Protein Assay. The recovered proteins were then subjected to Western blotting and COM crystal-protein binding assay.

COM crystal-protein binding assay

Apical membrane proteins were dialyzed against deionized water, lyophilized, and then resuspended in 1 ml of protein-free artificial urine, comprising 5 mM $CaCl_2$, 200 mM urea, 4 mM creatinine, 5 mM $Na_3C_6H_5O_7{\cdot}2H_2O$, 54 mM NaCl, 30 mM KCl, 15 mM NH_4Cl, 2 mM $MgSO_4{\cdot}7H_2O$, and 9 mM Na_2SO_4. Then, 5 mg of plain COM crystals were added to the protein solution and allowed binding at 4 °C on a continuous rotator for 16 h. Crystals with bound proteins were collected by centrifugation at 1500×*g* and 4 °C for 5 min and washed four times with 500 µl PBS and once with 500 µl of 5 mM EDTA prior to elution with Laemmli's buffer for subsequent Western blotting for PMCA2 (as described below). In parallel, the washed crystals (with proteins bound on the surface) were incubated with rabbit anti-PMCA2 (Abcam), isotype-controlled IgG (Sigma-Aldrich), or rabbit anti-gp135 (Millipore; Billerica MA, USA) antibody (all were diluted 1:100 in 1% BSA) at 37 °C for 1 h. After washing with PBS, the crystals were then incubated with Alexa546-conjugated goat anti-rabbit secondary antibody (1:500 in 1% BSA) at 37 °C for another 1 h. After the final wash with PBS, the presence of PMCA2 on the crystal surface was examined under ECLIPSE 80i fluorescence microscope (Nikon).

Western blotting

Proteins derived from IP (by both isotype-controlled IgG and anti-PMCA2 antibody) or COM crystal-protein binding assay along with positive controls (whole cell lysate and apical membrane protein fraction) were resolved by 10% SDS-PAGE and transferred onto nitrocellulose membrane using TE 77 PWR semi-dry transfer unit (GE Healthcare; Uppsala, Sweden) at 85 mA for 1.5 h. After blocking non-specific bindings with 5% skim milk in PBS at room temperature for 30 min, anti-PMCA2 primary antibody (1:1000 in 1% skim milk/PBS) was incubated with the membrane at 4 °C overnight. The membrane was further incubated with the corresponding secondary antibody conjugated with horseradish peroxidase (1:2000 in 1% skim milk/PBS) (Dako; Glostrup, Denmark) at room temperature for 1 h. The immunoreactive bands were then visualized by SuperSignal West Pico chemiluminescence substrate (Pierce Biotechnology, Inc.; Rockford, IL, USA) and autoradiography.

Neutralization of PMCA2 on the cell surface

MDCK cells were seeded in 6-well culture plate until confluency was reached. Culture medium was then removed and the cells were washed with membrane preserving buffer (1 mM $MgCl_2$ and 0.1 mM $CaCl_2$ in PBS). Non-specific bindings were blocked with 1% BSA in membrane preserving buffer for 15 min. Thereafter, the cells were washed with membrane preserving buffer three times and incubated with 1 µg/ml mouse monoclonal anti-PMCA2 antibody (Santa Cruz Biotechnology) or isotype-controlled IgG (Sigma-Aldrich; St. Louis, MO, USA) at 37 °C for 30 min. After washing with membrane preserving buffer, the cells were subjected to crystal-cell adhesion and crystal internalization assays as described below.

COM crystal-cell adhesion assay

Plain COM crystals (100 µg crystals/ml medium) were added onto the cell monolayer and incubated at 37 °C for 1 h. The unbound crystals were eliminated by five washes with PBS. Finally, the remaining adherent COM crystals on the cell monolayer were counted from 15 random high-power fields (HPFs) under a phase-contrast microscope (Eclipse Ti-S, Nikon; Tokyo, Japan).

COM crystal internalization assay

FITC-labeled COM crystals (1000 µg crystals/ml medium) were added onto the cell monolayer and allowed for internalization at 37 °C for 1 h. The unbound crystals were eliminated by five washes with PBS. Finally, the cells were incubated with 0.1% trypsin/2.5 mM EDTA in PBS to discard adhered but uninternalized crystals. The cells with internalized FITC-labeled COM crystals were then quantified by flow cytometry using BD Accuri™ C6 flow cytometer (Beckman Coulter; Fullerton, CA, USA).

Statistical analysis

All experiments were performed in three biological replicates, unless stated otherwise. Quantitative data are presented as mean ± SEM. One-way ANOVA followed by Tukey's post hoc test was performed for multiple comparisons of the data among groups. *p* values less than 0.05 were considered statistically significant.

Results

Analytical methods used in this study are summarized as a schematic in Fig. 1. An IP-MS approach was employed to isolate endogenous PMCA2 and to identify its interacting partners from MDCK cells. SDS-PAGE showed a distinct band at ~ 90 kDa only in the anti-PMCA2-IP samples in all triplicates (Fig. 2a). Western blotting confirmed that PMCA2 band was present only in the anti-PMCA2-IP sample indicating successful PMCA2 pull-down by IP (Fig. 2b). Each lane of the immunoprecipitated proteins derived from anti-PMCA2 or isotype-controlled IgG was excised into 20 gel slices (Fig. 2c) and subjected to in-gel tryptic digestion and

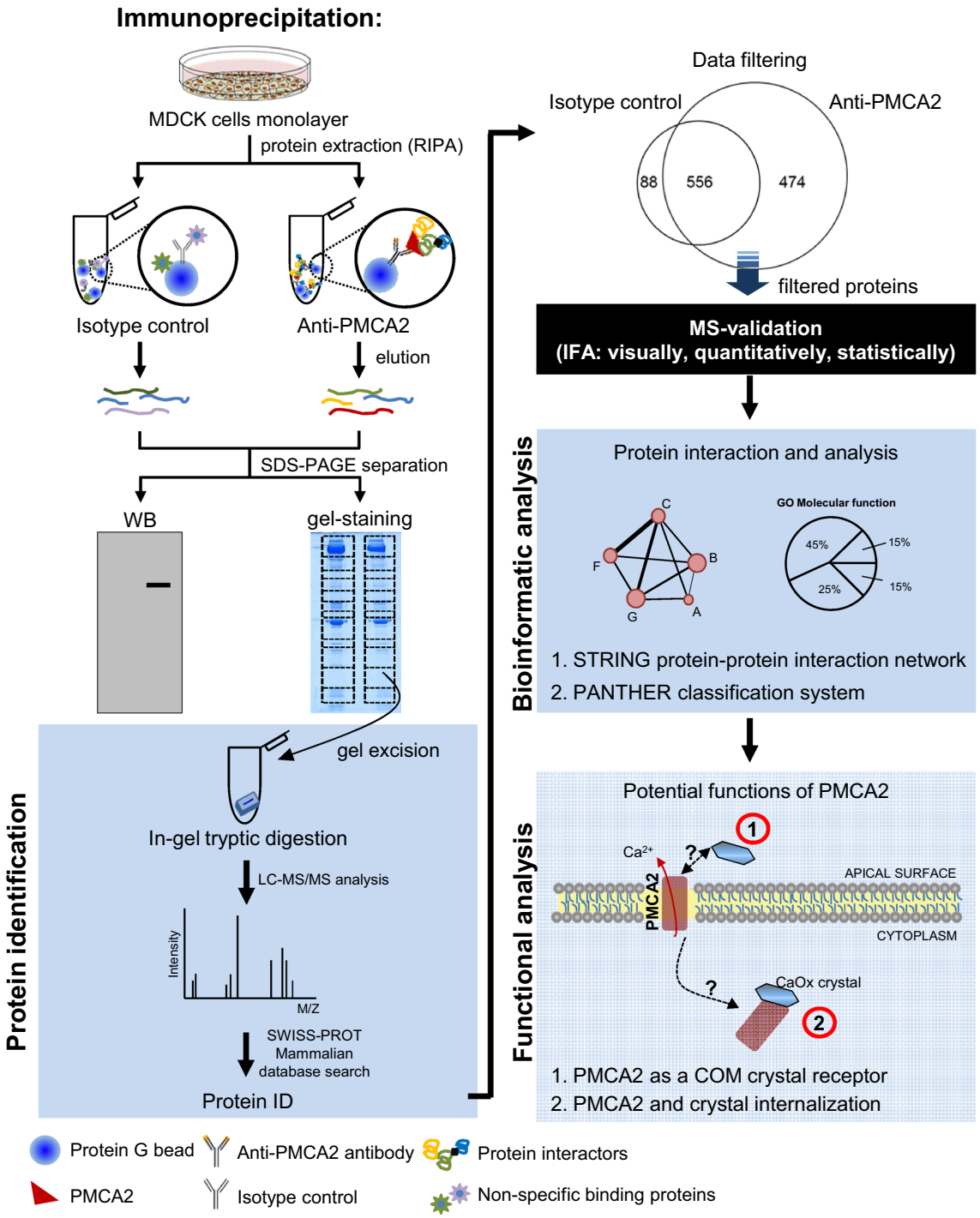

Fig. 1 Schematic for characterizations of PMCA2-interacting partners and its function

identified by nanoLC-ESI-Qq-TripleTOF MS/MS. Initially, IP-MS revealed a total of 1030 proteins in the anti-PMCA2-IP sample (Fig. 2d).

By eliminating "background contaminants" caused by non-specific bead/IgG bindings in the isotype-controlled sample, 644 non-specific binding proteins were excluded from the list (556 were common between anti-PMCA2-IP and isotype-controlled samples, whereas 88 were detected only in the isotype-controlled sample) (Fig. 2d). Finally, a total of 474 were defined as the PMCA2-interacting partners (Fig. 2d). Their identities and details of mass spectrometric data are summarized in Supplementary Table S1. As a confirmatory result, PMCA2 was one among those proteins in the PMCA2-interacting complex included in this list

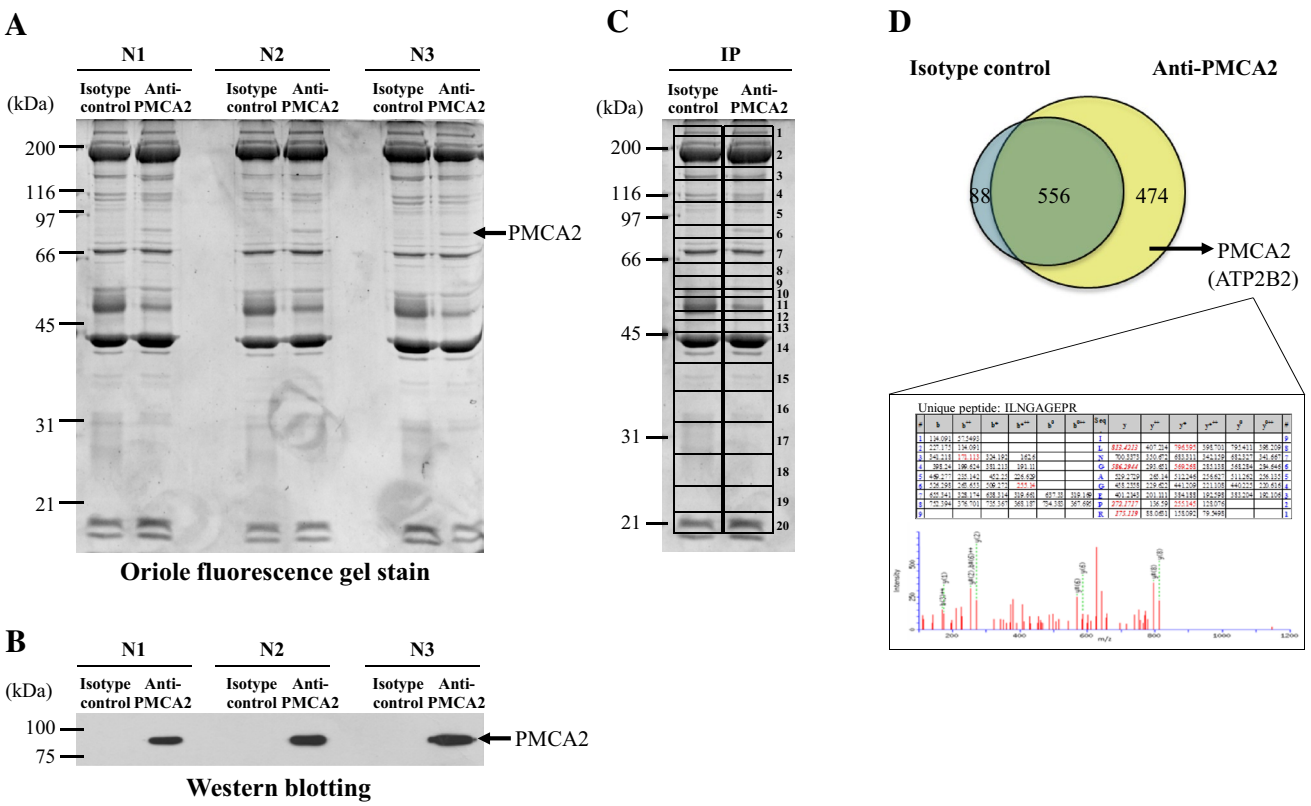

Fig. 2 IP-MS analysis of PMCA2-interacting complex. **a** Consistency of the SDS-PAGE band pattern of immunoprecipitated proteins in three independent experiments using anti-PMCA2 antibody vs. isotype-controlled IgG. **b** Western blotting to confirm the presence of PMCA2 in the immunoprecipitated samples. **c** Protein bands were excised to 20 gel slices/lane and subjected to in-gel tryptic digestion and identification by nanoLC-ESI-Qq-TripleTOF MS/MS. **d** A Venn diagram illustrating number of both specific and non-specific PMCA2 interactors. From a total of 1030 proteins identified in anti-PMCA2-IP sample, subtraction excluded 556 non-specific binders, leaving only 474 proteins to serve as potential PMCA2-interacting partners. The lower panel illustrates MS/MS spectra and fragmented ions of PMCA2 identified from nanoLC-ESI-Qq-TripleTOF MS/MS

(Fig. 2d, Table 1, and Supplementary Table S1). Among 474 PMCA2-interacting proteins identified, eight proteins were the known PMCA2 interactors, of which associations have been confirmed by experimental data [19, 32–34] (Table 1—part I). These included PDZ and LIM domain protein 7 [19], several calcineurin subunits [32], and protein kinase C (PKC) delta [33, 34].

STRING search tool was applied to classify the identified proteins by their likelihoods to serve as the PMCA2-interacting partners. Protein–protein interaction networks with a total input of 466 proteins (excluding eight known PMCA2 interactors as aforementioned) were computed based on the experimental data, literature evidence, and prediction from genomic context analysis [35]. The predicted networks were ranked by three confidence levels, including high confidence (score ≥ 0.70), medium confidence ($0.40 <$ score < 0.70), and low confidence ($0.15 <$ score ≤ 0.4) (Fig. 3). With the high confidence, no protein was predicted to be associated with PMCA2 (Table 1—part IIa). At the medium confidence, the prediction revealed four proteins associated with PMCA2 (Table 1—part IIb). With the low confidence, 16 were predicted to serve as potential PMCA2-interacting partners (Table 1—part IIc). Finally, proteins that were neither known nor potential PMCA2 interactors by such prediction were defined as the "novel PMCA2-interacting partners" (Table 1—part III).

The association of PMCA2 with its partners identified by IP-MS was validated by quantitative immuno-co-localization assay. Using this approach, we successfully confirmed the co-localization of PMCA2 with some of known PMCA2-interacting partners (ezrin and actin, which served as the positive controls) (Fig. 4a), potential PMCA2-interacting partners based on STRING analysis (Na^+/K^+-ATPase) (Fig. 4b), and novel PMCA2-interacting partners (annexin A1, Alix and hnRNP K) (Fig. 4c). The data showed no association of PMCA2 with non-PMCA2-interacting partners (c-Jun, SOD-1 and DJ-1, which served as the negative controls) (Fig. 4d).

PANTHER analysis revealed eight molecular functions of these PMCA2-interacting partners, including binding

Table 1 Summary of the PMCA2-interacting proteins identified by IP-MS

	Gene symbol	Protein name
I. Known PMCA2-interacting partners (with experimental evidence)		
*Ref. [19]	PDLIM7	PDZ and LIM domain protein 7
Ref. [32]	PPP2R2A	Serine/threonine-protein phosphatase 2A 55 kDa regulatory subunit B alpha isoform (calcineurin)
Ref. [32]	PPP2R1A	Serine/threonine-protein phosphatase 2A 65 kDa regulatory subunit A alpha isoform (calcineurin)
Ref. [32]	PPP6C	Serine/threonine-protein phosphatase 6 catalytic subunit (calcineurin)
Ref. [32]	PPP1CA	Serine/threonine-protein phosphatase PP1-alpha catalytic subunit (calcineurin)
Ref. [32]	PPP1CB	Serine/threonine-protein phosphatase PP1-beta catalytic subunit (calcineurin)
Ref. [32]	PPP1CC	Serine/threonine-protein phosphatase PP1-gamma catalytic subunit (calcineurin)
Refs. [33, 34]	PRKCD	Protein kinase C delta type
IIa. Potential PMCA2-interacting partners based on STRING analysis (high confidence: score ≥ 0.70)		
	–	– (None detected)
IIb. Potential PMCA2-interacting partners based on STRING analysis (medium confidence: 0.40 < score < 0.70)		
	ATP12A	Potassium-transporting ATPase alpha chain 2
	ATP1A2	Sodium/potassium-transporting ATPase subunit alpha-2
	ATP1A3	Sodium/potassium-transporting ATPase subunit alpha-3
	ATP1A4	Sodium/potassium-transporting ATPase subunit alpha-4
IIc. Potential PMCA2-interacting partners based on STRING analysis (low confidence: 0.15 < score ≤ 0.40)		
	DAPK1	Death-associated protein kinase 1 (calcium/calmodulin-dependent serine/threonine kinase)
	DAPK3	Death-associated protein kinase 3 (calcium/calmodulin-dependent serine/threonine kinase)
	EPHA2	Ephrin type-A receptor 2
#,*	GDI2	Rab GDP dissociation inhibitor 2
	MCU	Calcium uniporter protein, mitochondrial
	MOCS3	Adenylyltransferase and sulfurtransferase MOCS3
	MYL1	Myosin light chain 1/3, skeletal muscle isoform
	NKRF	NF-kappa-B-repressing factor
	NSF	Vesicle-fusing ATPase
	POTEF	POTE ankyrin domain family member F
	POTFJ	POTE ankyrin domain family member J
	RPS27A	Ubiquitin-40S ribosomal protein S27a
	TRIP13	Pachytene checkpoint protein 2 homolog
	UBB	Polyubiquitin-B
	UMPS	Uridine 5′-monophosphate synthase
	XPO1	Exportin-1
III. Novel PMCA2-interacting partners		
	YWHAQ	14-3-3 protein theta
	PSMC4	26S protease regulatory subunit 6B
	PSMC2	26S protease regulatory subunit 7
	PSMD13	26S proteasome non-ATPase regulatory subunit 13
	PSMD14	26S proteasome non-ATPase regulatory subunit 14
	PSMD3	26S proteasome non-ATPase regulatory subunit 3
	PSMD7	26S proteasome non-ATPase regulatory subunit 7
	OGDH	2-Oxoglutarate dehydrogenase, mitochondrial
	OGDHL	2-Oxoglutarate dehydrogenase-like, mitochondrial
	BCKDHB	2-Oxoisovalerate dehydrogenase subunit beta, mitochondrial
	RPSA	40S ribosomal protein SA
	PRKAA1	5′-AMP-activated protein kinase catalytic subunit alpha-1
	HSPD1	60 kDa heat shock protein, mitochondrial
	RPLP0	60S acidic ribosomal protein P0
	RPL10	60S ribosomal protein L10

Table 1 (continued)

	Gene symbol	Protein name
	RPL3	60S ribosomal protein L3
	RPL5	60S ribosomal protein L5
	RPL6	60S ribosomal protein L6
	ABI1	Abl interactor 1
	ABLIM3	Actin-binding LIM protein 3
	TRIP4	Activating signal cointegrator 1
	ACAD11	Acyl-CoA dehydrogenase family member 11
	SLC25A4	ADP/ATP translocase 1
	SLC25A31	ADP/ATP translocase 4
	AKAP8	A-kinase anchor protein 8
	ALDH7A1	Alpha-aminoadipic semialdehyde dehydrogenase
	CSN1S2A	Alpha-S2-casein-like A
	ALYREF2	Aly/REF export factor 2
	ACE2	Angiotensin-converting enzyme 2
	ANKEF1	Ankyrin repeat and EF-hand domain-containing protein 1
	ASB7	Ankyrin repeat and SOCS box protein 7
#	ANXA1	Annexin A1
	AP1B1	AP-1 complex subunit beta-1
	AP1M1	AP-1 complex subunit mu-1
	AP1M2	AP-1 complex subunit mu-2
	AP2B1	AP-2 complex subunit beta
	AP2M1	AP-2 complex subunit mu
	A1CF	APOBEC1 complementation factor
	GOT2	Aspartate aminotransferase, mitochondrial
	DARS	Aspartate–tRNA ligase, cytoplasmic
	ATAD3A	ATPase family AAA domain-containing protein 3A
	ATAD3B	ATPase family AAA domain-containing protein 3B
	ABCE1	ATP-binding cassette sub-family E member 1
	ABCF3	ATP-binding cassette sub-family F member 3
	ACLY	ATP-citrate synthase
	PFKP	ATP-dependent 6-phosphofructokinase, platelet type
	DDX1	ATP-dependent RNA helicase DDX1
	DDX39A	ATP-dependent RNA helicase DDX39A
	DHX8	ATP-dependent RNA helicase DHX8
	YME1L1	ATP-dependent zinc metalloprotease YME1L1
	EPB41L5	Band 4.1-like protein 5
	BZW2	Basic leucine zipper and W2 domain-containing protein 2
	ENO3	Beta-enolase
	EPRS	Bifunctional glutamate/proline–tRNA ligase
	MTHFD2	Bifunctional methylenetetrahydrofolate dehydrogenase/cyclohydrolase, mitochondrial
	BRCA2	Breast cancer type 2 susceptibility protein homolog
	BTBD9	BTB/POZ domain-containing protein 9
	BYSL	Bystin
	CAD	CAD protein
	CALU	Calumenin
	CTSZ	Cathepsin Z
	CCAR2	Cell cycle and apoptosis regulator protein 2
	CDC45	Cell division control protein 45 homolog
	CDC5L	Cell division cycle 5-like protein
	CDC123	Cell division cycle protein 123 homolog

Table 1 (continued)

	Gene symbol	Protein name
	CENPV	Centromere protein V
	CEP104	Centrosomal protein of 104 kDa
	CEP164	Centrosomal protein of 164 kDa
	CLIC1	Chloride intracellular channel protein 1
	CHAF1B	Chromatin assembly factor 1 subunit B
†	SNAP91	Clathrin coat assembly protein AP180
	CPSF3	Cleavage and polyadenylation specificity factor subunit 3
	CLPTM1	Cleft lip and palate transmembrane protein 1 homolog
	ARCN1	Coatomer subunit delta
	CCDC28A	Coiled-coil domain-containing protein 28A
	CCDC61	Coiled-coil domain-containing protein 61
	CHCHD3	Coiled-coil-helix-coiled-coil-helix domain-containing protein 3, mitochondrial
	COL4A2	Collagen alpha-2(IV) chain
	FAM120A	Constitutive coactivator of PPAR-gamma-like protein 1
	FAM120C	Constitutive coactivator of PPAR-gamma-like protein 2
	H2AFY	Core histone macro-H2A.1
	H2AFY2	Core histone macro-H2A.2
	CORO6	Coronin-6
	CUL1	Cullin-1
	CDK17	Cyclin-dependent kinase 17
	CDK20	Cyclin-dependent kinase 20
	CLNK	Cytokine-dependent hematopoietic cell linker
	CKAP2	Cytoskeleton-associated protein 2
	AGBL1	Cytosolic carboxypeptidase 4
	ALDH18A1	Delta-1-pyrroline-5-carboxylate synthase
	DNASE1L1	Deoxyribonuclease-1-like 1
	DGKB	Diacylglycerol kinase beta
	DLST	Dihydrolipoyllysine-residue succinyltransferase component of 2-oxoglutarate dehydrogenase complex, mitochondrial
	DPYS	Dihydropyrimidinase
	CRMP1	Dihydropyrimidinase-related protein 1
	DPYSL2	Dihydropyrimidinase-related protein 2
	MLH1	DNA mismatch repair protein Mlh1
	MSH2	DNA mismatch repair protein Msh2
	POLB	DNA polymerase beta
	MCM5	DNA replication licensing factor MCM5
	TOP2B	DNA topoisomerase 2-beta
	TOP1MT	DNA topoisomerase I, mitochondrial
	DNAJA1	DnaJ homolog subfamily A member 1
	DNAJA2	DnaJ homolog subfamily A member 2
	DNAJB12	DnaJ homolog subfamily B member 12
	DNAJC10	DnaJ homolog subfamily C member 10
	DNAJC11	DnaJ homolog subfamily C member 11
	DDOST	Dolichyl-diphosphooligosaccharide–protein glycosyltransferase 48 kDa subunit
	RPN1	Dolichyl-diphosphooligosaccharide–protein glycosyltransferase subunit 1
	RPN2	Dolichyl-diphosphooligosaccharide–protein glycosyltransferase subunit 2
	STAU1	Double-stranded RNA-binding protein Staufen homolog 1
	DBNL	Drebrin-like protein
	DSTYK	Dual serine/threonine and tyrosine protein kinase
	DYRK1A	Dual specificity tyrosine-phosphorylation-regulated kinase 1A

Table 1 (continued)

	Gene symbol	Protein name
	DYRK1B	Dual specificity tyrosine-phosphorylation-regulated kinase 1B
†	DNM3	Dynamin-3
	DST	Dystonin
	DTNA	Dystrobrevin alpha
	DTNB	Dystrobrevin beta
	RANBP2	E3 SUMO-protein ligase RanBP2
	TRIM39	E3 ubiquitin-protein ligase TRIM39
	TRIM56	E3 ubiquitin-protein ligase TRIM56
	UHRF1	E3 ubiquitin-protein ligase UHRF1
	EML4	Echinoderm microtubule-associated protein-like 4
†	EHD1	EH domain-containing protein 1
†	EHD2	EH domain-containing protein 2
†	EHD3	EH domain-containing protein 3
†	EHD4	EH domain-containing protein 4
	ELAVL4	ELAV-like protein 4
	ETFA	Electron transfer flavoprotein subunit alpha, mitochondrial
	EEF1A2	Elongation factor 1-alpha 2
	EEF1D	Elongation factor 1-delta
	EEF1G	Elongation factor 1-gamma
	ENDOD1	Endonuclease domain-containing 1 protein
	EPS8	Epidermal growth factor receptor kinase substrate 8
	EPS8L2	Epidermal growth factor receptor kinase substrate 8-like protein 2
	ERLIN1	Erlin-1
	ERLIN2	Erlin-2
	EIF4A3	Eukaryotic initiation factor 4A-III
	GSPT2	Eukaryotic peptide chain release factor GTP-binding subunit ERF3B
	EIF2S3	Eukaryotic translation initiation factor 2 subunit 3
	EIF2S3Y	Eukaryotic translation initiation factor 2 subunit 3, Y-linked
	EIF3B	Eukaryotic translation initiation factor 3 subunit B
	EIF3C	Eukaryotic translation initiation factor 3 subunit C
	EIF3D	Eukaryotic translation initiation factor 3 subunit D
	EIF3E	Eukaryotic translation initiation factor 3 subunit E
	DIS3	Exosome complex exonuclease RRP44
	XPO4	Exportin-4
	XPO7	Exportin-7
	XPOT	Exportin-T
	CAPZA2	F-actin-capping protein subunit alpha-2
	KHSRP	Far upstream element-binding protein 2
	FAF2	FAS-associated factor 2
	FAR1	Fatty acyl-CoA reductase 1
	FOLR2	Folate receptor beta
	FHL2	Four and a half LIM domains protein 2
	FMR1	Fragile X mental retardation protein 1
	FXR2	Fragile X mental retardation syndrome-related protein 2
	ALDOA	Fructose-bisphosphate aldolase A
	LGALS8	Galectin-8
	GMDS	GDP-mannose 4,6 dehydratase
	GMIP	GEM-interacting protein
	GLUD1	Glutamate dehydrogenase 1, mitochondrial
	GLUD2	Glutamate dehydrogenase 2, mitochondrial

Table 1 (continued)

	Gene symbol	Protein name
	GFPT1	Glutamine–fructose-6-phosphate aminotransferase [isomerizing] 1
	GFPT2	Glutamine–fructose-6-phosphate aminotransferase [isomerizing] 2
	QARS	Glutamine–tRNA ligase
	AGL	Glycogen debranching enzyme
	GTDC1	Glycosyltransferase-like domain-containing protein 1
	GOLGB1	Golgin subfamily B member 1
	GBF1	Golgi-specific brefeldin A-resistance guanine nucleotide exchange factor 1
	GRN	Granulins
	RAN	GTP-binding nuclear protein Ran
	GNAI1	Guanine nucleotide-binding protein G(i) subunit alpha-1
	GNB1	Guanine nucleotide-binding protein G(I)/G(S)/G(T) subunit beta-1
	GNAO1	Guanine nucleotide-binding protein G(o) subunit alpha
	GNAL	Guanine nucleotide-binding protein G(olf) subunit alpha
	GNAQ	Guanine nucleotide-binding protein G(q) subunit alpha
	GNAT1	Guanine nucleotide-binding protein G(t) subunit alpha-1
	GNA11	Guanine nucleotide-binding protein subunit alpha-11
	GNA14	Guanine nucleotide-binding protein subunit alpha-14
	GNA15	Guanine nucleotide-binding protein subunit alpha-15
	CLCN3	H(+)/Cl(−) exchange transporter 3
	CLCN5	H(+)/Cl(−) exchange transporter 5
	DKC1	H/ACA ribonucleoprotein complex subunit 4
	HHIP	Hedgehog-interacting protein
	HNF1B	Hepatocyte nuclear factor 1-beta
#	HNRNPA1L2	Heterogeneous nuclear ribonucleoprotein A1-like 2
	HNRNPD	Heterogeneous nuclear ribonucleoprotein D0
	HNRNPH2	Heterogeneous nuclear ribonucleoprotein H2
	HNRNPK	Heterogeneous nuclear ribonucleoprotein K
	HNRNPL	Heterogeneous nuclear ribonucleoprotein L
	HK1	Hexokinase-1
	HK2	Hexokinase-2
	HK3	Hexokinase-3
	KAT2B	Histone acetyltransferase KAT2B
	HDAC1	Histone deacetylase 1
	HDAC2	Histone deacetylase 2
	HIST1H1A	Histone H1.1
	HIST1H1C	Histone H1.2
	HIST1H1D	Histone H1.3
	HIST1H1T	Histone H1t
	H2AFX	Histone H2AX
	H2BFS	Histone H2B type F-S
	H3F3C	Histone H3.3C
	RBBP4	Histone-binding protein RBBP4
	RBBP7	Histone-binding protein RBBP7
	KMT2A	Histone-lysine *N*-methyltransferase 2A
	HMBOX1	Homeobox-containing protein 1
	KPNB1	Importin subunit beta-1
	IGF2BP1	Insulin-like growth factor 2 mRNA-binding protein 1
	IGF2BP2	Insulin-like growth factor 2 mRNA-binding protein 2
	IGF2BP3	Insulin-like growth factor 2 mRNA-binding protein 3
	ITGA2	Integrin alpha-2 (fragment)

Table 1 (continued)

	Gene symbol	Protein name
	ITGB4	Integrin beta-4
	IFIT2	Interferon-induced protein with tetratricopeptide repeats 2
	IDH3B	Isocitrate dehydrogenase (NAD) subunit beta, mitochondrial
	KLHDC7A	Kelch domain-containing protein 7A
	KEAP1	Kelch-like ECH-associated protein 1
	KLHL7	Kelch-like protein 7
	KLHL9	Kelch-like protein 9
	KHDRBS1	KH domain-containing, RNA-binding, signal transduction-associated protein 1
	KIF12	Kinesin-like protein KIF12
	KIF13B	Kinesin-like protein KIF13B
	KIF1A	Kinesin-like protein KIF1A
	KIF1B	Kinesin-like protein KIF1B
	KIF1C	Kinesin-like protein KIF1C
	KIF20A	Kinesin-like protein KIF20A
	KIF2B	Kinesin-like protein KIF2B
	KIF2C	Kinesin-like protein KIF2C
	KIFC1	Kinesin-like protein KIFC1
	LMNB2	Lamin-B2
	LCA5L	Lebercilin-like protein
	LZTS1	Leucine zipper putative tumor suppressor 1
	LZTS3	Leucine zipper putative tumor suppressor 3
	LRCH1	Leucine-rich repeat and calponin homology domain-containing protein 1
	LRCH2	Leucine-rich repeat and calponin homology domain-containing protein 2
	LRGUK	Leucine-rich repeat and guanylate kinase domain-containing protein
	LRRC59	Leucine-rich repeat-containing protein 59
	LPPR1	Lipid phosphate phosphatase-related protein type 1
	ACSL3	Long-chain-fatty-acid–CoA ligase 3
	ACSL4	Long-chain-fatty-acid–CoA ligase 4
	HELLS	Lymphoid-specific helicase
	KDM7A	Lysine-specific demethylase 7A
	LYG2	Lysozyme g-like protein 2
	MVP	Major vault protein
	MARK3	MAP/microtubule affinity-regulating kinase 3
	MELK	Maternal embryonic leucine zipper kinase
	PAQR8	Membrane progestin receptor beta
#	MTA1	Metastasis-associated protein MTA1
	MTA2	Metastasis-associated protein MTA2
	MTA3	Metastasis-associated protein MTA3
	MARS	Methionine–tRNA ligase, cytoplasmic
	MCCC2	Methylcrotonoyl-CoA carboxylase beta chain, mitochondrial
	MINK1	Misshapen-like kinase 1
#,*	SLC25A22	Mitochondrial glutamate carrier 1
#,*	SLC25A18	Mitochondrial glutamate carrier 2
†	RHOT1	Mitochondrial Rho GTPase 1
	MAP4K4	Mitogen-activated protein kinase kinase kinase kinase 4
	BUB3	Mitotic checkpoint protein BUB3
	MISP	Mitotic interactor and substrate of PLK1
	NIFK	MKI67 FHA domain-interacting nucleolar phosphoprotein
	SMAD2	Mothers against decapentaplegic homolog 2
	SMAD3	Mothers against decapentaplegic homolog 3

Table 1 (continued)

	Gene symbol	Protein name
	SMAD9	Mothers against decapentaplegic homolog 9
	MYD88	Myeloid differentiation primary response protein MyD88
	NAT10	*N*-acetyltransferase 10
	NCKIPSD	NCK-interacting protein with SH3 domain
	NBEAL2	Neurobeachin-like protein 2
	NEFL	Neurofilament light polypeptide
	NAV3	Neuron navigator 3
	NPY5R	Neuropeptide Y receptor type 5
	FAM129B	Niban-like protein 1
	NCBP1	Nuclear cap-binding protein subunit 1
	NUFIP2	Nuclear fragile X mental retardation-interacting protein 2
	NUP93	Nuclear pore complex protein Nup93
	NCOA5	Nuclear receptor coactivator 5
	YBX1	Nuclease-sensitive element-binding protein 1
	NOL6	Nucleolar protein 6
	UBTF	Nucleolar transcription factor 1
	TIAL1	Nucleolysin TIAR
	NPM1	Nucleophosmin
	OR6N2	Olfactory receptor 6N2
	OAT	Ornithine aminotransferase, mitochondrial
	CDC73	Parafibromin
	PCID2	PCI domain-containing protein 2
	GIPC1	PDZ domain-containing protein GIPC1
	PCM1	Pericentriolar material 1 protein
†	PICALM	Phosphatidylinositol-binding clathrin assembly protein
	PGM3	Phosphoacetylglucosamine mutase
#	ATP2B2	Plasma membrane calcium-transporting ATPase 2
	PAPOLA	Poly(A) polymerase alpha
	PAPOLB	Poly(A) polymerase beta
	PCBP3	Poly(rC)-binding protein 3
	PABPC1L	Polyadenylate-binding protein 1-like
	PABPC4L	Polyadenylate-binding protein 4-like
	POLDIP3	Polymerase delta-interacting protein 3
	PTBP2	Polypyrimidine tract-binding protein 2
	PTBP3	Polypyrimidine tract-binding protein 3
	PRPF19	Pre-mRNA-processing factor 19
	DDX20	Probable ATP-dependent RNA helicase DDX20
	DDX4	Probable ATP-dependent RNA helicase DDX4
	DDX47	Probable ATP-dependent RNA helicase DDX47
	SETX	Probable helicase senataxin
	RBM46	Probable RNA-binding protein 46
†	PDCD6IP	Programmed cell death 6-interacting protein (Alix)
	PCNA	Proliferating cell nuclear antigen
	AGO2	Protein argonaute-2
	CYR61	Protein CYR61
	FAM83B	Protein FAM83B
	PRRC2A	Protein PRRC2A
	RCC2	Protein RCC2
	TBRG4	Protein TBRG4
	TFG	Protein TFG

Table 1 (continued)

	Gene symbol	Protein name
	SEC23B	Protein transport protein Sec23B
	ZYG11B	Protein zyg-11 homolog B
	LOX	Protein-lysine 6-oxidase
	NPEPPSL1	Puromycin-sensitive aminopeptidase-like protein
	HSP90B2P	Putative endoplasmin-like protein
	EIF2S3L	Putative eukaryotic translation initiation factor 2 subunit 3-like protein
#	HSPA7	Putative heat shock 70 kDa protein 7
#	HSP90AA2	Putative heat shock protein HSP 90-alpha A2
#	HSP90AA5P	Putative heat shock protein HSP 90-alpha A
#	HSP90AB4P	Putative heat shock protein HSP 90-beta 4
	DHX16	Putative pre-mRNA-splicing factor ATP-dependent RNA helicase DHX16
	PDHB	Pyruvate dehydrogenase E1 component subunit beta, mitochondrial
	RAB11FIP1	Rab11 family-interacting protein 1
	RACGAP1	Rac GTPase-activating protein 1
	RAF1	RAF proto-oncogene serine/threonine-protein kinase
	RALBP1	RalA-binding protein 1
	RANGAP1	Ran GTPase-activating protein 1
	G3BP1	Ras GTPase-activating protein-binding protein 1
	G3BP2	Ras GTPase-activating protein-binding protein 2
	IQGAP1	Ras GTPase-activating-like protein IQGAP1
†	RAC1	Ras-related C3 botulinum toxin substrate 1
†	RAC3	Ras-related C3 botulinum toxin substrate 3
†	RAB1A	Ras-related protein Rab-1A
	RAB26	Ras-related protein Rab-26
	RAB37	Ras-related protein Rab-37
	RAB39B	Ras-related protein Rab-39B
#,*,†	RAB5A	Ras-related protein Rab-5A
	RCC1	Regulator of chromosome condensation
	RFC2	Replication factor C subunit 2
	RFC4	Replication factor C subunit 4
	RFC5	Replication factor C subunit 5
	RPA1	Replication protein A 70 kDa DNA-binding subunit
	RTKN	Rhotekin
	RRM1	Ribonucleoside-diphosphate reductase large subunit
	BOP1	Ribosome biogenesis protein BOP1
	RCL1	RNA 3′-terminal phosphate cyclase-like protein
	RBM47	RNA-binding protein 47
	RALY	RNA-binding protein Raly
	CROCC	Rootletin
	RUVBL1	RuvB-like 1
	RUVBL2	RuvB-like 2
	MAT1A	*S*-adenosylmethionine synthase isoform type-1
	MAT2A	*S*-adenosylmethionine synthase isoform type-2
	SEPT10	Septin-10
	SEPT11	Septin-11
	SEPT14	Septin-14
	SEPT6	Septin-6
	SEPT7	Septin-7
	SEPT8	Septin-8
	SEPT9	Septin-9

Table 1 (continued)

	Gene symbol	Protein name
	SQSTM1	Sequestosome-1
	SHMT2	Serine hydroxymethyltransferase, mitochondrial
	SRSF2	Serine/arginine-rich splicing factor 2
	SRSF8	Serine/arginine-rich splicing factor 8
	ARAF	Serine/threonine-protein kinase A-Raf
	BRAF	Serine/threonine-protein kinase B-raf
	MARK1	Serine/threonine-protein kinase MARK1
	MARK2	Serine/threonine-protein kinase MARK2
	CDC42BPB	Serine/threonine-protein kinase MRCK beta
	NEK5	Serine/threonine-protein kinase Nek5
	PAK2	Serine/threonine-protein kinase PAK 2
	PLK1	Serine/threonine-protein kinase PLK1
	SH3BP4	SH3 domain-binding protein 4
	SNRPN	Small nuclear ribonucleoprotein-associated protein N
	SMTN	Smoothelin
	SNW1	SNW domain-containing protein 1
	SLC2A1	Solute carrier family 2, facilitated glucose transporter member 1
	SLC22A4	Solute carrier family 22 member 4
†	SNX2	Sorting nexin-2
	STRBP	Spermatid perinuclear RNA-binding protein
	DDX39B	Spliceosome RNA helicase DDX39B
	SF3B2	Splicing factor 3B subunit 2
	SFPQ	Splicing factor, proline- and glutamine-rich
	CTTN	Src substrate cortactin
	SRPK1	SRSF protein kinase 1
	STOML3	Stomatin-like protein 3
	SMC2	Structural maintenance of chromosomes protein 2
	SDHA	Succinate dehydrogenase (ubiquinone) flavoprotein subunit, mitochondrial
	SUN2	SUN domain-containing protein 2
	SKIV2L2	Superkiller viralicidic activity 2-like 2
	VAT1	Synaptic vesicle membrane protein VAT-1 homolog
	SYTL3	Synaptotagmin-like protein 3
	STXBP2	Syntaxin-binding protein 2
	TLN1	Talin-1
	TARDBP	TAR DNA-binding protein 43
	TPX2	Targeting protein for Xklp2
	TBPL2	TATA box-binding protein-like protein 2
	TAX1BP1	Tax1-binding protein 1 homolog
	CCT2	T-complex protein 1 subunit beta
	CCT7	T-complex protein 1 subunit eta
	CCT6A	T-complex protein 1 subunit zeta
	CCT6B	T-complex protein 1 subunit zeta-2
	TES	Testin
†	TOM1L2	TOM1-like protein 2
	TNIK	TRAF2 and NCK-interacting protein kinase
	TTF2	Transcription termination factor 2
	TBL3	Transducin beta-like protein 3
	TKTL1	Transketolase-like protein 1
	SSR1	Translocon-associated protein subunit alpha
	TNPO3	Transportin-3

Table 1 (continued)

	Gene symbol	Protein name
	HADHB	Trifunctional enzyme subunit beta, mitochondrial
	RTCB	tRNA-splicing ligase RtcB homolog
	TMOD1	Tropomodulin-1
	TMOD2	Tropomodulin-2
	TUBAL3	Tubulin alpha chain-like 3
	TUBA3A	Tubulin alpha-3 chain
#	TUBB2A	Tubulin beta-2A chain
#	N/A	Tubulin beta-8 chain-like protein LOC260334
	TUBG1	Tubulin gamma-1 chain
	TUBG2	Tubulin gamma-2 chain
	TP53I13	Tumor protein p53-inducible protein 13
	HCK	Tyrosine-protein kinase HCK
	JAK1	Tyrosine-protein kinase JAK1
	UTP15	U3 small nucleolar RNA-associated protein 15 homolog
	UTP18	U3 small nucleolar RNA-associated protein 18 homolog
	PRPF3	U4/U6 small nuclear ribonucleoprotein Prp3
	USP26	Ubiquitin carboxyl-terminal hydrolase 26
	USP7	Ubiquitin carboxyl-terminal hydrolase 7
	UBA1	Ubiquitin-like modifier-activating enzyme 1
	N/A	Uncharacterized protein C2orf57 homolog
	MYO1H	Unconventional myosin-Ih
	UMOD	Uromodulin
	UTS2	Urotensin-2
	VPS26A	Vacuolar protein sorting-associated protein 26A
	VPS35	Vacuolar protein sorting-associated protein 35
	VASP	Vasodilator-stimulated phosphoprotein
	VTN	Vitronectin
	VDAC1	Voltage-dependent anion-selective channel protein 1
	ATP6V1A	V-type proton ATPase catalytic subunit A
	WDR1	WD repeat-containing protein 1
	XRCC5	X-ray repair cross-complementing protein 5
	YTHDF2	YTH domain-containing family protein 2

N/A not applicable

*Different protein isoforms were reported in previous research articles. However, these isoforms exhibit similar function(s)

#Identified as COM crystal-binding proteins in our previous study [31]

†Identified as proteins involved in endocytosis pathway

(38.9%), catalytic (34.0%), receptor (9.7%), transcription factor (5.6%), transporter (4.2%), enzyme regulator (3.6%), translation regulator (3.4%), and structural molecule (0.6%) activities (Fig. 5a). Further stratification of the binding activity, which was the most prominent function, showed nucleic acid binding (48.9%), protein binding (37.9%), and calcium ion binding (7.8%) as the top-three subgroups. This was consistent with the data reported in our previous large-scale proteomic study demonstrating that PMCA2 isolated from apical membranes of MDCK renal tubular cells was one among the COM crystal-binding proteins [31]. However, such previous proteomic screening had not been validated. This present study thus addressed the potential role of PMCA2 as a COM crystal-binding protein. Expression of PMCA2 in MDCK whole cell as well as apical membranes and COM crystal-binding fraction was confirmed by Western blotting. As shown in Fig. 5b, immunoreactive band of PMCA2 was detectable in whole cell lysate, apical membrane fraction, and COM crystal-bound fraction, confirming the role of PMCA2 as a COM crystal-binding protein. Moreover, immunofluorescence staining clearly showed PMCA2 on the surface of COM crystals after COM crystal-protein binding assay, which further strengthened its role as the COM crystal-binding protein (Fig. 5c).

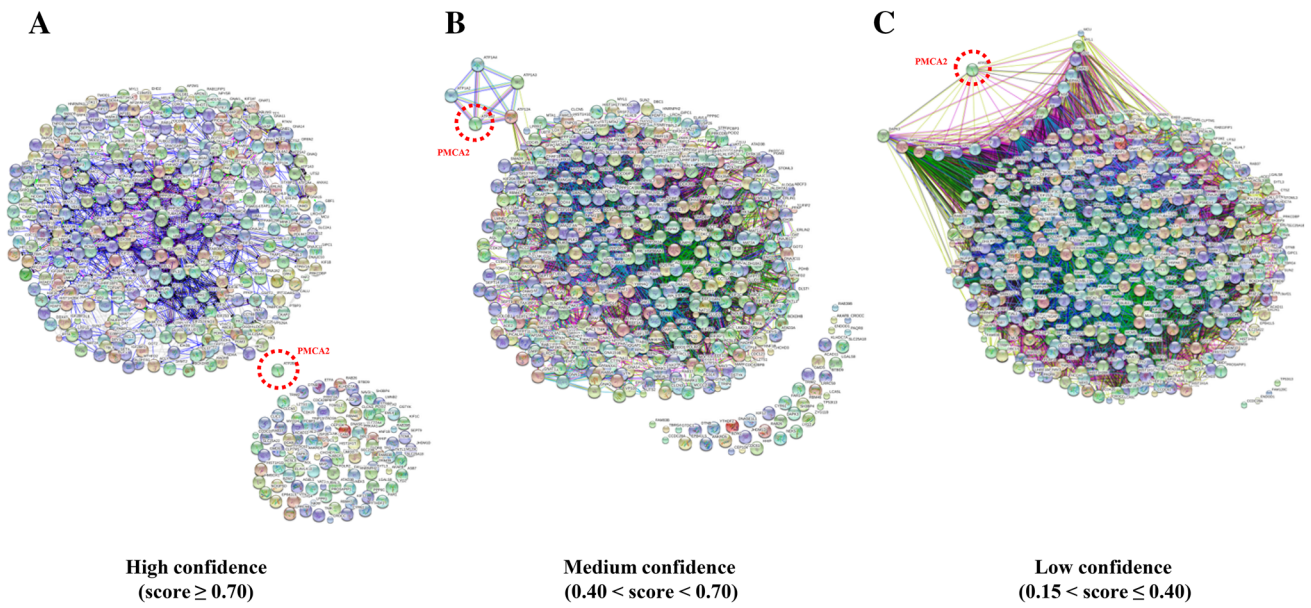

Fig. 3 Protein–protein interactions networks of PMCA2-interacting partners. Interaction networks of 474 unique proteins associated with PMCA2 were computed by STRING software to predict the likelihood being the PMCA2-interacting partners based on confidence level. **a** High confidence (score ≥ 0.70). **b** Medium confidence (0.40 < score < 0.70). **c** Low confidence (0.15 < score ≤ 0.40). PMCA2 encoded by *ATP2B2* gene is highlighted in a red-dotted circle. Only protein nodes that displayed direct interactions to PMCA2 are reported as potential PMCA2-interacting proteins in Table 1 (parts IIa–IIc)

The functional role of PMCA2 as a potential COM crystal receptor was further validated by crystal-cell adhesion assay on the intact MDCK cells. Analysis of the controlled cells indicated that COM crystals could bind to the cells (Fig. 6a, b). Neutralization of surface PMCA2 expression by a specific anti-PMCA2 antibody dramatically reduced the number of adherent crystals from 28.0 ± 3.4 to 18.1 ± 2.5 (no./HPF) as compared to the blank control, whereas neutralization by the isotype-controlled IgG had no significant effects (Fig. 6a, b). This data confirmed the role of PMCA2 as a potential COM crystal receptor. Moreover, the role of PMCA2 in COM crystal internalization into the cells was investigated using FITC-labeled crystals followed by flow cytometry. While the controlled cells showed the internalized/endocytotic crystals, neutralization of the surface PMCA2 by a specific anti-PMCA2 antibody dramatically reduced the number of internalized crystals from 19.26 ± 0.01 to 13.56 ± 0.02% as compared to the blank control (Fig. 6c, d). There was no significant change observed when the isotype-controlled IgG was used for neutralization (Fig. 6c, d).

Discussion

The aim of this study was to characterize PMCA2-interacting partners in distal renal tubular cells hoping to gain insights into novel functions of PMCA2. IP-MS was our method of choice to identify affinity-purified proteins because of its capability to detect low abundant proteins and novel protein partners. To eliminate background contaminants caused by non-specific bindings of proteins to IgG or beads that are frequently co-purified in the IP samples, up-front reduction of such contaminants was done during experiments (i.e., by pre-clearing and vigorous washes). Additionally, post-experimental elimination of contaminants (i.e., using highly stringent criteria for MS/MS analysis and subtraction with the isotype-controlled IgG pulled down proteins) was also performed to further discriminate true interactors from non-specific binders.

From a total of 474 proteins identified as the potential PMCA2-interacting proteins, it should be noted that we were unable to detect some of the known PMCA2 interactors. For example, sodium–hydrogen exchange regulatory factor 2 (NHERF2) that has been previously reported as an interactor of PMCA2 in MDCK cells [15, 36] was not found in the present study. This was likely due to the fact that protein–protein interactions naturally do not present in equal stoichiometry [37]. NHERF2 might exhibit a specific but lower abundance and/or lower affinity towards PMCA2, resulting to an increase of risk for protein loss during isolation or purification steps. In addition, interaction between NHERF2 and PMCA2 might be transient (they might be associated only during specific stimuli, cell stage, or signaling events; thereby increasing the difficulty to be isolated and identified by IP-MS) [38]. Another potential factor recognized as experimental limitation that had led to the loss of specific

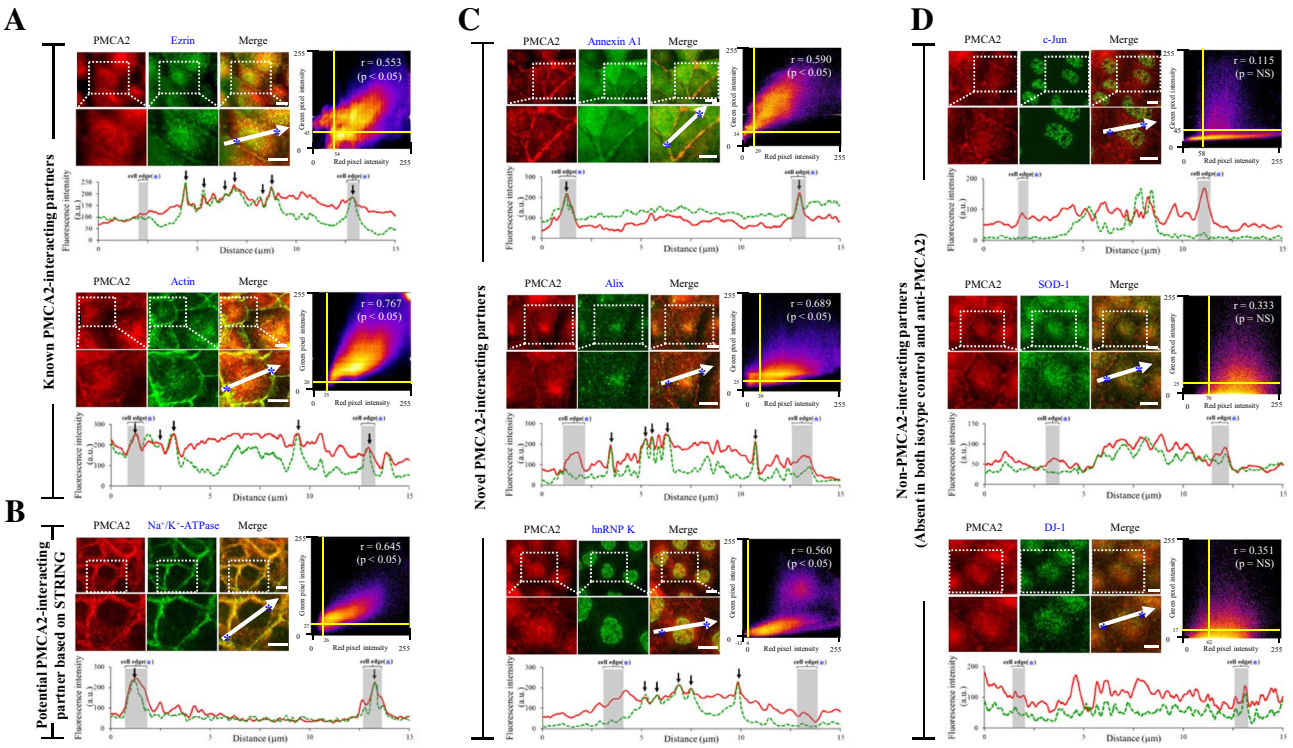

Fig. 4 Quantitative immuno-co-localization analysis of PMCA2 and its interacting partners. **a** PMCA2 vs. known PMCA2-interacting partners (ezrin and actin) (served as the positive controls). **b** PMCA2 vs. potential PMCA2-interacting partners based on STRING analysis (Na^+/K^+-ATPase). **c** PMCA2 vs. novel PMCA2-interacting partners (annexin A1, Alix and hnRNP K). **d** PMCA2 vs. non-PMCA2-interacting partners (c-Jun, SOD-1 and DJ-1) (served as the negative controls). In each pair, intensity correlation scatter plot estimated the degree of co-localization between red (PMCA2) and green (protein partner of interest) signals. Pixel intensity thresholds are indicated with yellow lines. Pearson's correlation coefficient (*r*) of the co-localization is shown in the top-right corner of the plot. Intensity profile of the two immunofluorescence signals along the linear section of area of interest (indicated with white arrow) at a distance of 15 μm across the cell is depicted at the bottom of each pair. PMCA2 is displayed as a red line, whereas the partner protein of interest is displayed in green-dotted line. Area of the cell edge (plasma membrane) is labeled with an asterisk and highlighted in gray. Co-localization of the two probes is indicated with black arrow. A scale bar represents 5-μm-distance

partners was through an over-filtering of the data. Ideally, all proteins presented in the isotype-controlled sample were considered as "background contaminants" and were eventually eliminated. However, some true interactors could, in fact, also bind non-specifically to the beads. This inevitably resulted in the loss of specific binding partners; as evidenced by the removal of ezrin and actin (the known interactors of PMCA2 [15, 39]) from the final list of PMCA2-interacting partners (Table 1). This has been proven by quantitative immuno-co-localization assay (Fig. 4a).

Nevertheless, at least eight genuine PMCA2-associated proteins were identified in this study. These included PDZ and LIM domain protein 7 [19], several calcineurin subunits [32], and PKC delta [33, 34] (Table 1—part I). PDZ/LIM domain protein and PKC are the important activators/modulators that have been found to bind to a consensus sequence at C-terminal tail of all PMCA isoforms [19]. On the other hand, the interaction between calcineurin and PMCA is isoform-specific [32]. Previous evidence have demonstrated that calcineurin interacted very strongly to PMCA2 and only weakly with PMCA4 in human breast adenocarcinoma cells [32]. Moreover, we successfully identified the heterodimerized form of calcineurin, which consisted of catalytic subunit calcineurin A and Ca^{2+}-binding subunit calcineurin B [40], suggesting functionally active form of calcineurin could be also detected by our approach. These supported the validity of the IP-MS data as proteins in the list were likely to be selective towards PMCA2.

To conceptualize these identified PMCA2-interacting complex in a more meaningful manner, STRING software was utilized. The protein–protein interaction networks provided by STRING combined several lines of evidence (through experiments, databases and text mining) to include all possible interactions. Therefore, the interaction networks predicted in the present study provided almost complete overview of these proteins' associations (Fig. 3). However, it should be kept in mind that these PMCA2-interacting partners might correspond to the ones that interacted directly

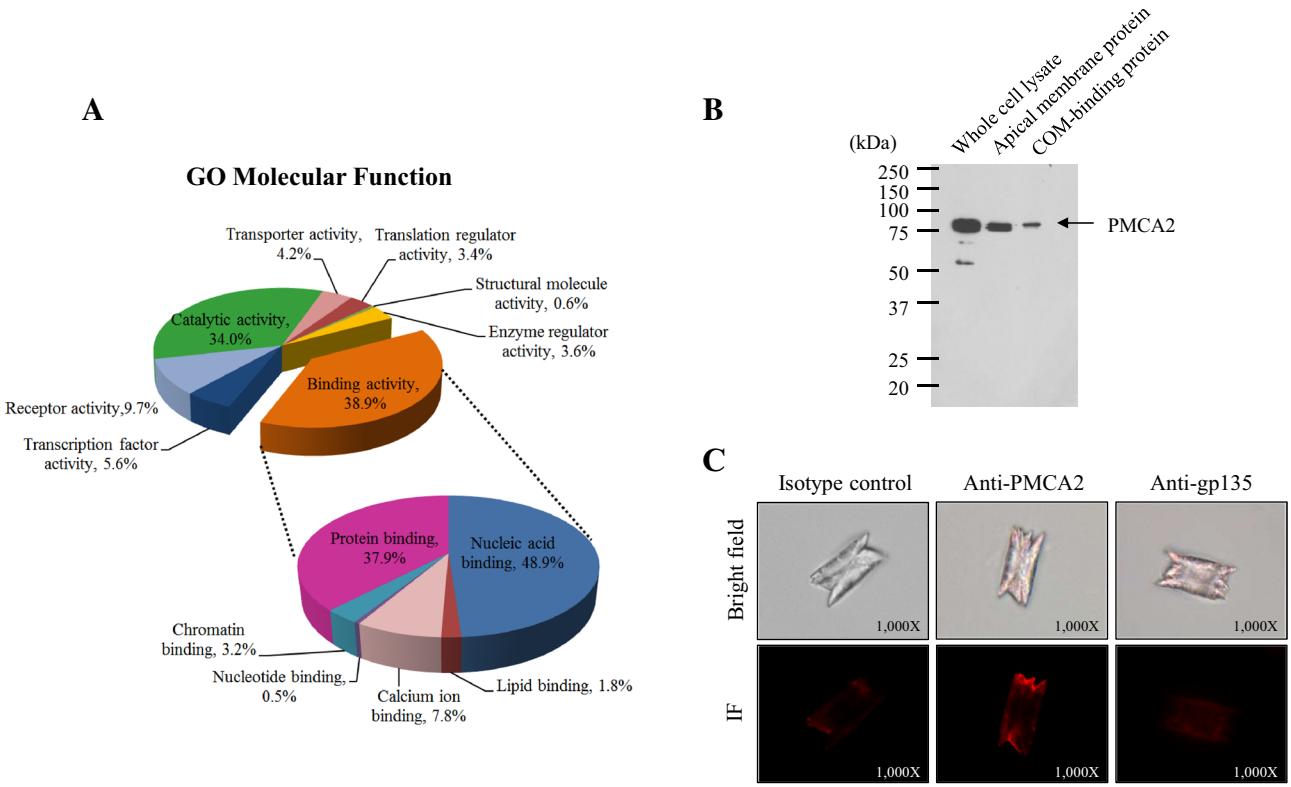

Fig. 5 Gene ontology (GO) analysis of PMCA2-interacting partners and a novel role of PMCA2 as a COM crystal-binding protein. **a** GO classification by molecular function using PANTHER database showed eight potential functions of PMCA2 interactors, especially binding activity, which is the most predominant one (38.9%). Further breakdown of the binding activity is shown as a zoom-in pie chart. **b** COM crystal-protein binding assay followed by Western blotting to confirm the presence of PMCA2 in whole cell lysate, apical membranes, and COM crystal-bound fraction. **c** COM crystal-protein binding assay followed by immunofluorescence (IF) staining using anti-PMCA2 primary antibody to confirm the presence of PMCA2 (in red) on the crystal surface, whereas staining with isotype-controlled IgG and anti-gp135 antibody served as the negative controls (original magnification was ×1000)

with PMCA2, as well as those that interacted indirectly via one or more bridging molecules (e.g., other proteins, RNA, etc.) [41].

The most prominent molecular function of all identified proteins was binding activity. Interestingly, a large number of Ca^{2+}-binding proteins were identified in this study (approximately 7.8% of all identified proteins with binding activity; Fig. 5a). Ca^{2+} homeostasis in distal renal tubular cells is predominantly controlled by two specialized transporters, NCX and PMCA. NCX (with a low Ca^{2+}-binding affinity) can facilitate the removal of a large amount of Ca^{2+} out of the cells within a short period. This is beneficial when the cells need to get rid of excessive Ca^{2+} ions after an encounter of a sudden rise of intracellular Ca^{2+} concentration [42]. In contrast, PMCA is responsible for fine-tuning the intracellular Ca^{2+} level. It has been recognized as a low-capacity but high-affinity pump that interacts with Ca^{2+} even when the surrounding concentration of Ca^{2+} is extremely low [5]. PMCA2, in particular, carries a unique feature in which its activity at the basal level is as high as when its activator (calmodulin) is present [7]. Moreover, PMCA2 has a high Ca^{2+}-binding affinity when compared to other isoforms expressed in MDCK cells [7].

These properties have raised the possibility that PMCA2 may be involved in the pathogenesis of calcium nephrolithiasis. Recent kidney stone research had been intensively conducted to define mechanisms of adhesion of causative crystals on renal cells that subsequently lead to crystal retention/deposition and finally stone formation [43, 44]. Studies of COM crystals, the most common constituent found in human kidney stones have shown that crystal attachment onto renal tubular cells depends largely on charge interaction between cellular surface molecules and the crystals [45, 46]. We thus have postulated that an interaction between COM crystals, on which cationic sites are formed by Ca^{2+} ions and PMCA2 at apical surface of renal tubular cells, serves as a critical initiating event that promotes crystal retention.

To address this hypothesis, an initial step was taken to find a correlation between PMCA2 and crystal deposition by comparing PMCA2-interacting proteins to a list of COM crystal-binding proteins recently reported [31]. Approximately 22% of COM crystal-binding proteins

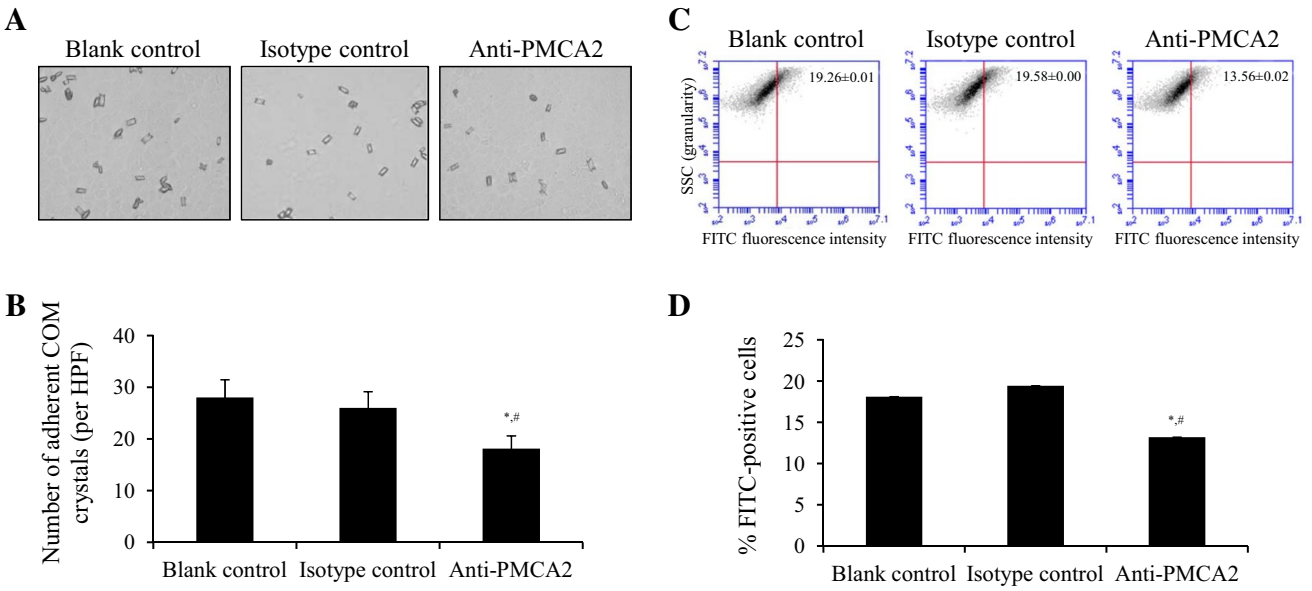

Fig. 6 Functional validation of the role of PMCA2 in COM crystal-cell adhesion and crystal internalization. **a** Phase-contrast microscopic examination after crystal-cell adhesion assay together with neutralization using specific anti-PMCA2 antibody compared to isotype-controlled IgG and blank control (original magnification power was ×400). **b** Quantitative data were obtained from 15 randomized HPFs and are presented as mean ± SEM of three independent experiments. **c** Dot plot analysis of side scatter (SSC) or granularity (*y*-axis) and FITC-fluorescence intensity (*x*-axis) of the cells after crystal neutralization assay together with neutralization using specific anti-PMCA2 antibody compared to isotype-controlled IgG and blank control. **d** Quantitative data (percentages of the cells with internalized crystals) were obtained from three independent experiments and are presented as mean ± SEM. $^{*}p < 0.05$ vs. blank control; $^{\#}p < 0.05$ vs. isotype-controlled IgG

identified in previous study also served as the PMCA2 interactors (Note that the COM crystal-binding proteins are marked with # in Table 1). Further validation at experimental level by COM crystal-protein binding assay confirmed that PMCA2 served as a COM crystal-binding protein (Fig. 5b, c). We have also shown that PMCA2 is expressed at the apical membranes of MDCK renal tubular cells (Fig. 5b). The localization of PMCA2 at the apical membranes suggested the likelihood of interaction between PMCA2 and COM crystals in physiological condition as crystal deposition occurs inside the tubular lumen where the apical part of epithelial cells is facing. Thus, the role of PMCA2 as a potential receptor on the cell surface to bind with COM crystals was confirmed by crystal-cell adhesion assay together with antibody neutralization (Fig. 6a, b). Our previous studies have also shown that the adherent COM crystals could be internalized into the cells by surface receptors through lipid raft-mediated endocytosis pathway [47, 48]. Similarly, apical membrane localization of PMCA2 is lipid raft-dependent [12], implicating its possible role in mediating COM crystal uptake by endocytosis. The data obtained from IP-MS in the present study supported this hypothesis as there were several proteins involved in vesicle-mediated transport and endocytosis pathway included in the list (marked with † in Table 1). Finally, the role of PMCA2 in crystal internalization into the cells was confirmed experimentally by crystal internalization assay (Fig. 6c, d).

In conclusion, we report herein a large number of PMCA2-interacting proteins, most of which have not been previously reported and can serve as the novel PMCA2-interacting partners. Also, our findings have reinforced the functional versatility of PMCA2 enhanced by different arrays of specific protein interactions and are the first dataset to link PMCA2 to the pathogenesis of kidney stone disease through direct binding to COM crystals as a potential COM crystal receptor that plays role in crystal uptake into renal tubular cells.

Acknowledgements We thank Phornpimon Tipthara and Kedsarin Fong-ngern for their technical assistance. This study was supported by Mahidol University research grant, Office of the Higher Education Commission and Mahidol University under the National Research Universities Initiative, and the Thailand Research Fund (IRN60W0004 and IRG5980006). AV is supported by Siriraj Graduate Thesis Scholarship, whereas VT is supported by "Research Staff" Grant.

Author contributions AV and VT designed research; AV performed experiments; AV and VT analyzed data; AVand VT wrote the manuscript; all authors reviewed the manuscript.

Compliance with ethical standards

Conflict of interest The authors declare no conflict of interest.

References

1. Strehler EE, Zacharias DA (2001) Role of alternative splicing in generating isoform diversity among plasma membrane calcium pumps. Physiol Rev 81:21–50
2. Schuh K, Uldrijan S, Gambaryan S, Roethlein N, Neyses L (2003) Interaction of the plasma membrane Ca^{2+} pump 4b/CI with the Ca^{2+}/calmodulin-dependent membrane-associated kinase CASK. J Biol Chem 278:9778–9783
3. Carafoli E (1991) Calcium pump of the plasma membrane. Physiol Rev 71:129–153
4. Oberleithner H, Westphale HJ, Gassner B (1991) Alkaline stress transforms Madin-Darby canine kidney cells. Pflug Arch 419:418–420
5. Strehler EE, Filoteo AG, Penniston JT, Caride AJ (2007) Plasma-membrane Ca(2+) pumps: structural diversity as the basis for functional versatility. Biochem Soc Trans 35:919–922
6. Strehler EE, Caride AJ, Filoteo AG, Xiong Y, Penniston JT, Enyedi A (2007) Plasma membrane Ca^{2+} ATPases as dynamic regulators of cellular calcium handling. Ann N Y Acad Sci 1099:226–236
7. Domi T, Di Leva F, Fedrizzi L, Rimessi A, Brini M (2007) Functional specificity of PMCA isoforms? Ann N Y Acad Sci 1099:237–246
8. Lee WJ, Roberts-Thomson SJ, Monteith GR (2005) Plasma membrane calcium-ATPase 2 and 4 in human breast cancer cell lines. Biochem Biophys Res Commun 337:779–783
9. Spiden SL, Bortolozzi M, Di Leva F, de Angelis MH, Fuchs H, Lim D, Ortolano S, Ingham NJ, Brini M, Carafoli E, Mammano F, Steel KP (2008) The novel mouse mutation Oblivion inactivates the PMCA2 pump and causes progressive hearing loss. PLoS Genet 4:e1000238
10. Schultz JM, Yang Y, Caride AJ, Filoteo AG, Penheiter AR, Lagziel A, Morell RJ, Mohiddin SA, Fananapazir L, Madeo AC, Penniston JT, Griffith AJ (2005) Modification of human hearing loss by plasma-membrane calcium pump PMCA2. N Engl J Med 352:1557–1564
11. Kurnellas MP, Nicot A, Shull GE, Elkabes S (2005) Plasma membrane calcium ATPase deficiency causes neuronal pathology in the spinal cord: a potential mechanism for neurodegeneration in multiple sclerosis and spinal cord injury. FASEB J 19:298–300
12. Xiong Y, Antalffy G, Enyedi A, Strehler EE (2009) Apical localization of PMCA2w/b is lipid raft-dependent. Biochem Biophys Res Commun 384:32–36
13. Kip SN, Strehler EE (2004) Vitamin D3 upregulates plasma membrane Ca^{2+}-ATPase expression and potentiates apicobasal Ca^{2+} flux in MDCK cells. Am J Physiol Ren Physiol 286:F363–F369
14. Friedman PA (2000) Mechanisms of renal calcium transport. Exp Nephrol 8:343–350
15. Padanyi R, Xiong Y, Antalffy G, Lor K, Paszty K, Strehler EE, Enyedi A (2010) Apical scaffolding protein NHERF2 modulates the localization of alternatively spliced plasma membrane Ca^{2+} pump 2B variants in polarized epithelial cells. J Biol Chem 285:31704–31712
16. Kip SN, Strehler EE (2003) Characterization of PMCA isoforms and their contribution to transcellular Ca^{2+} flux in MDCK cells. Am J Physiol Ren Physiol 284:F122–F132
17. Lopreiato R, Giacomello M, Carafoli E (2014) The plasma membrane calcium pump: new ways to look at an old enzyme. J Biol Chem 289:10261–10268
18. Brini M (2009) Plasma membrane Ca(2+)-ATPase: from a housekeeping function to a versatile signaling role. Pflug Arch 457:657–664
19. Strehler EE (2013) Plasma membrane calcium ATPases as novel candidates for therapeutic agent development. J Pharm Pharm Sci 16:190–206
20. Gingras AC, Gstaiger M, Raught B, Aebersold R (2007) Analysis of protein complexes using mass spectrometry. Nat Rev Mol Cell Biol 8:645–654
21. Dukes JD, Whitley P, Chalmers AD (2011) The MDCK variety pack: choosing the right strain. BMC Cell Biol 12:43
22. Sritippayawan S, Chiangjong W, Semangoen T, Aiyasanon N, Jaetanawanitch P, Sinchaikul S, Chen ST, Vasuvattakul S, Thongboonkerd V (2007) Proteomic analysis of peritoneal dialysate fluid in patients with different types of peritoneal membranes. J Proteome Res 6:4356–4362
23. Havanapan PO, Thongboonkerd V (2009) Are protease inhibitors required for gel-based proteomics of kidney and urine? J Proteome Res 8:3109–3117
24. Bolte S, Cordelieres FP (2006) A guided tour into subcellular colocalization analysis in light microscopy. J Microsc 224:213–232
25. Dunn KW, Kamocka MM, McDonald JH (2011) A practical guide to evaluating colocalization in biological microscopy. Am J Physiol Cell Physiol 300:C723–C742
26. Thongboonkerd V, Semangoen T, Chutipongtanate S (2006) Factors determining types and morphologies of calcium oxalate crystals: molar concentrations, buffering, pH, stirring and temperature. Clin Chim Acta 367:120–131
27. Thongboonkerd V, Semangoen T, Sinchaikul S, Chen ST (2008) Proteomic analysis of calcium oxalate monohydrate crystal-induced cytotoxicity in distal renal tubular cells. J Proteome Res 7:4689–4700
28. Chaiyarit S, Mungdee S, Thongboonkerd V (2010) Non-radioactive labelling of calcium oxalate crystals for investigations of crystal-cell interaction and internalization. Anal Methods 2:1536–1541
29. Chaiyarit S, Singhto N, Thongboonkerd V (2016) Calcium oxalate monohydrate crystals internalized into renal tubular cells are degraded and dissolved by endolysosomes. Chem Biol Interact 246:30–35
30. Fong-ngern K, Chiangjong W, Thongboonkerd V (2009) Peeling as a novel, simple, and effective method for isolation of apical membrane from intact polarized epithelial cells. Anal Biochem 395:25–32
31. Fong-ngern K, Peerapen P, Sinchaikul S, Chen ST, Thongboonkerd V (2011) Large-scale identification of calcium oxalate monohydrate crystal-binding proteins on apical membrane of distal renal tubular epithelial cells. J Proteome Res 10:4463–4477
32. Holton M, Yang D, Wang W, Mohamed TM, Neyses L, Armesilla AL (2007) The interaction between endogenous calcineurin and the plasma membrane calcium-dependent ATPase is isoform specific in breast cancer cells. FEBS Lett 581:4115–4119
33. Kosk-Kosicka D, Zylinska L (1997) Protein kinase C and calmodulin effects on the plasma membrane Ca^{2+}-ATPase from excitable and nonexcitable cells. Mol Cell Biochem 173:79–87
34. Usachev YM, DeMarco SJ, Campbell C, Strehler EE, Thayer SA (2002) Bradykinin and ATP accelerate Ca(2+) efflux from rat sensory neurons via protein kinase C and the plasma membrane Ca(2+) pump isoform 4. Neuron 33:113–122
35. Szklarczyk D, Franceschini A, Wyder S, Forslund K, Heller D, Huerta-Cepas J, Simonovic M, Roth A, Santos A, Tsafou KP, Kuhn M, Bork P, Jensen LJ, von Mering C (2015) STRING v10: protein–protein interaction networks, integrated over the tree of life. Nucleic Acids Res 43:D447–D452
36. DeMarco SJ, Chicka MC, Strehler EE (2002) Plasma membrane Ca^{2+} ATPase isoform 2b interacts preferentially with Na^+/H^+ exchanger regulatory factor 2 in apical plasma membranes. J Biol Chem 277:10506–10511

37. Perkins JR, Diboun I, Dessailly BH, Lees JG, Orengo C (2010) Transient protein–protein interactions: structural, functional, and network properties. Structure 18:1233–1243
38. Boulon S, Ahmad Y, Trinkle-Mulcahy L, Verheggen C, Cobley A, Gregor P, Bertrand E, Whitehorn M, Lamond AI (2010) Establishment of a protein frequency library and its application in the reliable identification of specific protein interaction partners. Mol Cell Proteom 9:861–879
39. Bozulic LD, Malik MT, Powell DW, Nanez A, Link AJ, Ramos KS, Dean WL (2007) Plasma membrane Ca(2+)-ATPase associates with CLP36, alpha-actinin and actin in human platelets. Thromb Haemost 97:587–597
40. Rusnak F, Mertz P (2000) Calcineurin: form and function. Physiol Rev 80:1483–1521
41. von Mering C, Krause R, Snel B, Cornell M, Oliver SG, Fields S, Bork P (2002) Comparative assessment of large-scale data sets of protein–protein interactions. Nature 417:399–403
42. Carafoli E, Santella L, Branca D, Brini M (2001) Generation, control, and processing of cellular calcium signals. Crit Rev Biochem Mol Biol 36:107–260
43. Dardamanis M (2013) Pathomechanisms of nephrolithiasis. Hippokratia 17:100–107
44. Vinaiphat A, Thongboonkerd V (2017) Prospects for proteomics in kidney stone disease. Expert Rev Proteom 14:185–187
45. Lieske JC, Leonard R, Toback FG (1995) Adhesion of calcium oxalate monohydrate crystals to renal epithelial cells is inhibited by specific anions. Am J Physiol 268:F604–F612
46. Lieske JC, Leonard R, Swift H, Toback FG (1996) Adhesion of calcium oxalate monohydrate crystals to anionic sites on the surface of renal epithelial cells. Am J Physiol 270:F192–F199
47. Kanlaya R, Sintiprungrat K, Chaiyarit S, Thongboonkerd V (2013) Macropinocytosis is the major mechanism for endocytosis of calcium oxalate crystals into renal tubular cells. Cell Biochem Biophys 67:1171–1179
48. Fong-ngern K, Sueksakit K, Thongboonkerd V (2016) Surface heat shock protein 90 serves as a potential receptor for calcium oxalate crystal on apical membrane of renal tubular epithelial cells. J Biol Inorg Chem 21:463–474